Chemical Engineering Journal 466 (2023) 143346

Contents lists available at ScienceDirect

Chemical Engineering Journal

journal homepage: www.elsevier.com/locate/cej

Experimental and computational studies of the production of 1,3-butadiene from 2,3-butanediol using SiO_2-supported H_3PO_4 derivatives

Juan V. Alegre-Requena [a,b,*], Glenn R. Hafenstine [c], Xiangchen Huo [c], Yanfei Guan [a], Jim Stunkel [c], Frederick G. Baddour [c], Kinga A. Unocic [d], Bruno C. Klein [c], Ryan E. Davis [c], Robert S. Paton [a], Derek R. Vardon [c,*], Seonah Kim [a,c,*]

[a] Department of Chemistry, Colorado State University, Fort Collins, CO 80523, USA
[b] Departamento de Química Inorgánica, Instituto de Síntesis Química y Catálisis Homogénea (ISQCH) CSIC-Universidad de Zaragoza, Zaragoza 50009, Spain
[c] National Bioenergy Center, National Renewable Energy Laboratory, Golden, CO 80401, USA
[d] Center for Nanophase Materials Sciences, Oak Ridge National Laboratory, Oak Ridge, TN 37831, USA

ARTICLE INFO

Keywords:
Butadiene
2,3-butanediol
Computational chemistry
QM/MM
Heterogeneous catalysis
H_3PO_4 derivatives
Mechanistic studies

ABSTRACT

Silica-supported phosphoric acid and metal phosphate catalyzed 1,3-butadiene (**BDE**) production from 2,3-butanediol (**2,3-BDO**) was studied using experimental and computational techniques. The catalyst was initially tested in a continuous flow reactor using commercially available **2,3-BDO**, leading to maximum **BDE** yields of 63C%. Quantum chemical mechanistic studies revealed 1,2-epoxybutane is a kinetically viable and thermodynamically stable intermediate, supported by experimental demonstration that this epoxide can be converted to **BDE** under standard reaction conditions. Newly proposed E2 and S_N2' elementary steps were studied to rationalize the formation of **BDE** and all detected side-products. Additionally, using quantum mechanics/molecular mechanics (QM/MM) calculations, we modeled silica-supported phosphate catalysts to study the effect of the alkali metal center. Natural population analysis showed that phosphate oxygen atoms are more negatively charged in CsH_2PO_4/SiO_2 than in H_3PO_4/SiO_2. In combination with temperature-programmed desorption experiments using CO_2, the results of this study suggest that the improved selectivity achieved when adding the metal center is related to an increase in the basicity of the catalyst.

1. Introduction

1,3-Butadiene (**BDE**) is a prolific building block for the chemical industry,[1,2] widely used in polymerization processes to produce synthetic rubbers, elastomers, and polymer resins.[3–5] Polymers derived from **BDE** are ubiquitous in manufacturing materials, such as tires, which have a tremendous worldwide economic impact. Promoted by the diminishing availability of fossil fuels and the adverse environmental effects of non-renewable resources, new and efficient syntheses of **BDE** from renewable feedstocks have attracted considerable attention within the scientific community.[1] 2,3-butanediol (**2,3-BDO**) is one such promising precursor since it can be obtained from sugars by microbial fermentation in over 90% yield[6–8] and, subsequently, can be converted into **BDE** by catalytic dehydration using silica-supported H_3PO_4 (H_3PO_4/SiO_2) derivatives.[9,10] Of the catalytic systems in these studies, mono-metallic hydrogen phosphates (i.e., MH_2PO_4) give the highest selectivities for the desired product, especially when using CsH_2PO_4/SiO_2 as the catalyst.

When comparing to other catalysts that use **2,3-BDO** as the starting material, the CsH_2PO_4 system is amongst the optimal catalysts in terms of reactivity and selectivity, showing > 85% **BDE** yield in flow reactors at 400 °C and performing better than other metal phosphates.[9] Rare earth phosphates ($NdPO_4$) have also been employed at 280–330 °C, showing inferior catalytic performances (47% BDE selectivity).[11] Alternative types of catalysts, such as metal oxides, have also shown to catalyze **BDE** production from **2,3-BDO**, albeit with lower efficiency. For example, Sc_2O_3[12] led to 80% **BDE** yields at 400 °C, and Al_2O_3[13] to 55% **BDE** selectivity at 400 °C with low conversions. More elaborated double-bed catalysts containing Sc_2O_3 and Al_2O_3 have also been employed to raise **BDE** yield to 94%.[14] Additionally, zeolites such as

* Corresponding authors at: Department of Chemistry, Colorado State University, Fort Collins, CO 80523, USA; Departamento de Química Inorgánica, Instituto de Síntesis Química y Catálisis Homogénea (ISQCH) CSIC-Universidad de Zaragoza, Zaragoza 50009, Spain; National Bioenergy Center, National Renewable Energy Laboratory, Golden, CO 80401, USA.
E-mail addresses: jv.alegre@csic.es (J.V. Alegre-Requena), dvardon@alderfuels.com (D.R. Vardon), seonah.kim@colostate.edu (S. Kim).

https://doi.org/10.1016/j.cej.2023.143346
Received 27 January 2023; Received in revised form 16 April 2023; Accepted 2 May 2023
Available online 8 May 2023

HZSM-5(280) and HY(60) have catalyzed these dehydrations, but the resulting **BDE** yields (<20%) were significantly lower than those observed for MH_2PO_4 derivatives.[15] The abundance of contributions in this field serves as evidence for the importance of utilizing supported catalysts to convert biomass-derived precursors, offering a promising green approach for industrial **BDE** production that circumvents the need for petroleum derivatives.

Greater mechanistic understanding of MH_2PO_4/SiO_2-catalyzed production of **BDE** from **2,3-BDO** has the potential to address current bottlenecks associated with conversion and selectivity for the desired product. Detailed mechanistic and computational studies have not been performed to date, although key intermediates have been proposed (Fig. 1).[9,10] For example, the secondary carbocation **B2OL**$^+$ is currently assumed to play a central role in the mechanism via an E1 elimination; however, secondary aliphatic carbocations are notably unstable (especially in the gas phase).[16,17] In this work, besides the previously proposed pathways, alternative steps such as E2 reactions, substitutions, and other related chemical transformations were considered in computational mechanistic studies, and ultimately found to be more stable. Additionally, a leading hypothesis has suggested that the size of the alkali metal (in metal phosphate catalysts) influences product selectivity through steric effects.[9] However, electronic parameters typically also affect catalytic properties (i.e., basicity or acidity) and, therefore, we contrasted both possibilities in the theoretical study.

In this work, we combine experimental studies, quantum mechanics (QM) and quantum mechanics/molecular mechanics (QM/MM)[18–20] calculations to critically evaluate a wide range of possible reaction pathways that can take place during the catalytic process. Multiple types of elimination (E1 and E2) and substitution (S_N2 and S_N2') elementary steps were included to create a more complex mechanistic picture. Additionally, the role of the Cs center was closely inspected by considering potential electronic and steric effects that can influence the selectivity and reactivity of the process. Catalysts based upon H_3PO_4/SiO_2 functionalities were synthesized and characterized to determine the distribution and activity of the active phase. Overall, this combination of theory and experiment enables tailored catalyst development for improving selectivity and stability following logical approaches rather than trial and error protocols.

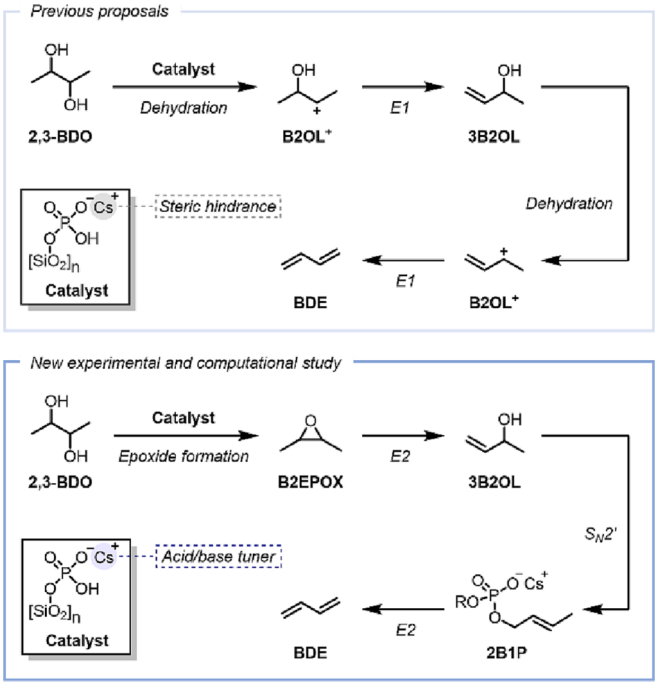

Fig. 1. Previous and revised mechanistic proposals for CsH_2PO_4/SiO_2-catalyzed **BDE** formation.

2. Result and discussion

2.1. Validation of CsH_2PO_4/SiO_2 for BDE production

To experimentally evaluate **BDE** production from **2,3-BDO**, a supported CsH_2PO_4 catalyst was synthesized due to its reported high selectivity for **BDE**. An H_3PO_4 catalyst was prepared for comparison.[9] The catalysts were synthesized using a conventional impregnation method and commercial SiO_2 with a high surface area. Catalyst samples were stored under dry nitrogen after calcination to minimize water adsorption, since previous reports have shown that conversion with water occurs rapidly at room temperature.[21,22] The loading of CsH_2PO_4 was designed to achieve 10 wt% of CsH_2PO_4 (5.13 wt% Cs based upon precursor masses) on SiO_2, which reduced the catalyst surface area by ~ 30% without significant change of pore volume (Fig. 2, bottom). A detailed study carried out by Filimonov and coworkers suggests that there are different factors for this effect, including the acidity and basicity of the catalytic units, the nature of the metal center, and the weight proportion of the catalyst.[10].

Further characterization by STEM-EDS showed that both Cs and P were uniformly distributed across the SiO_2 support without forming large agglomerates (Fig. 2, top). Additionally, ^{31}P MAS NMR spectroscopy was performed on CsH_2PO_4/SiO_2 and H_3PO_4/SiO_2 to determine the distribution of phosphate moieties in each catalyst. ^{31}P NMR analysis of CsH_2PO_4/SiO_2 revealed three spectroscopic features that could be assigned to monophosphate (0.5 ppm), terminal/monophosphate (-8.9 ppm), and 2-coordinate phosphate species (–22.2 ppm) (Fig. S1).[23–28] Peak fitting of these features suggests that most of the phosphate species deposited onto the surface exist as mono- or pyrophosphate groups. Similarly, ^{31}P NMR analysis of H_3PO_4/SiO_2 revealed the same primary peaks, with the addition of a broad shoulder at –37 ppm that could be attributed to 3-coordinate phosphate species. Additionally, H_3PO_4/SiO_2 possessed a relatively higher abundance of polymeric phosphate with 25.3% of the observed signal corresponding to multi-coordinated internal phosphates. By comparison, only 4.9% of the phosphorus in the CsH_2PO_4/SiO_2 catalyst was dually coordinated. A further 23.8 % of the phosphorus appeared as pyrophosphate and monophosphate groups with slight ppm shifts in CsH_2PO_4/SiO_2, which we attribute to Cs coordination.

The CsH_2PO_4/SiO_2 catalyst was first tested for **2,3-BDO** dehydration to validate its ability for **BDE** production in a packed-bed reactor. The mass of **2,3-BDO** fed to the reactor and gas-phase production of **BDE** were monitored to calculate the **BDE** yield. At 400 °C, which was the optimal temperature reported previously for high **2,3-BDO** conversion (>99.9%) and **BDE** selectivity (>85%) in a previous study,[9] **BDE** yield

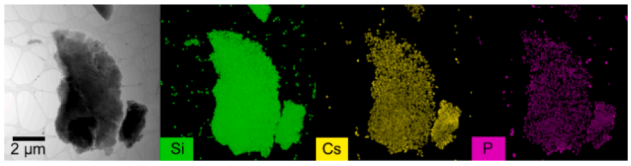

Catalyst	Loading (wt%)[a]		BET surface area ($m^2\ g^{-1}$)	Pore V ($cm^3\ g^{-1}$)
	Cs	P		
SiO_2	-	-	480	0.75
CsH_2PO_4/SiO_2	5.13	1.07	337	0.76
H_3PO_4/SiO_2	-	1.18	480	0.91

Fig. 2. Top: STEM image and EDS elemental maps (Si, Cs and P) of CsH_2PO_4/SiO_2. Bottom: Cs and P loadings, surface area, and pore volume of supported phosphate catalysts. [a] Determined by ICP.

achieved a maximum value of 59 carbon % (C%) and slowly decreased with time-on-stream afterward (Fig. 3). The recovery of condensable products is shown in Fig. S2. The initial **BDE** yield was slightly increased to 63C% by increasing the temperature from 400 °C to 425 °C, however, higher temperatures were not employed since the proportion of side-products becomes significant as seen previously.[9] These values are more closely aligned with the **BDE** yields reported recently by Kim *et al.* [10].

Quantification of **2,3-BDO** conversion was hindered by incomplete mass recovery (75% from both tests). Similar incomplete carbon balances have been observed previously when using CsH_2PO_4/SiO_2 catalysts.[10] Considering that this study utilized a combination of gas-phase analytical and gravimetric measurements similar to that reported in the literature,[9] the lower mass recovery and **BDE** yield observed here may suggest that dehydration of pure **2,3-BDO** is sensitive to the reactor design and operation. Specifically, the separation system requires careful design to separate the condensable effluents (e.g., unreacted **2,3-BDO**, H_2O, oxygenate products) for gravimetric measurements from the hydrocarbon products for online analysis. As an illustration, a dehydration test of *n*-butanol was performed with the CsH_2PO_4/SiO_2 catalyst to assess the impact of product portfolio on mass recovery. Under the same reaction conditions as **2,3-BDO** dehydration, the *n*-butanol dehydration test achieved 98% mass recovery, which can be attributed to the efficient separation between the hydrocarbon product (butene, boiling point of −4.4 °C) and the condensable effluents (predominantly unreacted *n*-butanol and H_2O, boiling points of 117.7 °C and 100 °C, respectively) (Fig. S3). Most studies that achieved high carbon balance for **2,3-BDO** dehydration employed online gas chromatography to quantify all organic compounds.[15,29–32] However, procedures that only measure gas-phase products may not effectively quantify the H_2O side-product. Oligomerization of **BDE** and different side-products downstream of the reactor has also been proposed as problematic to mass recovery and long-term operation.[10,31,33] Possible solutions include co-feeding water [13,33] or varying partial pressure and residence time with diluent gasses.[10,33] Nonetheless,

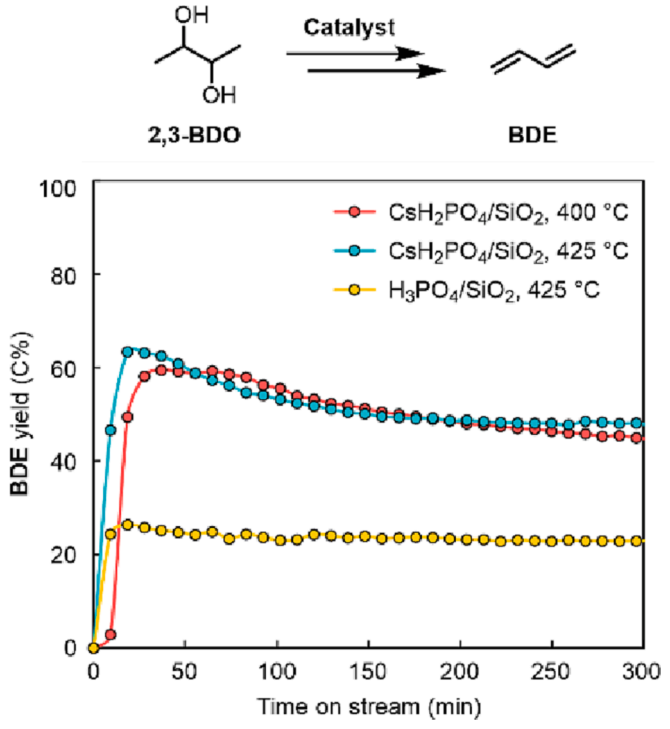

Fig. 3. **BDE** production from **2,3-BDO** at different conditions using 2.0 g catalyst, 0.017 g/min **2,3-BDO** and 1 atm He (containing 10% v/v Ar as an internal standard) at 60 cm^3 (STP) min^{-1}.

BDE was verified to be the major product from **2,3-BDO** dehydration with the CsH_2PO_4/SiO_2 catalyst, consistent with literature reports.

To evaluate the impact of Cs on product selectivity, the H_3PO_4/SiO_2 catalyst was tested for **2,3-BDO** dehydration (Fig. 3). Under the same reaction conditions, **BDE** yield remained relatively constant and significantly lower than the **BDE** yield observed with the CsH_2PO_4/SiO_2 catalyst (maximum yield of 26 vs 63C% and turnover frequency after 20 min of 0.06 vs 0.17 min^{-1}), confirming the role of Cs in promoting **BDE** formation.

2.2. Mechanistic studies of BDE production

QM[34–38] calculations were used to interrogate the mechanism, based on experience studying related extended catalytic systems, such as silica and zeolites.[39–44] A reduced QM model using H_3PO_4 as the catalyst was initially employed to consider multiple elementary steps and many substrate ground (GS) and transition state (TS) conformers, which would be challenging with electronic structure calculations employing periodic boundary conditions.[45–48] Dehydration of hydrogen phosphates to form metaphosphates, $(MPO_3)_n$, may occur under the reaction conditions employed, and for this reason, alternative catalyst models of the active site were studied computationally. The conclusions obtained when using these derivatives are analogous to those obtained with the H_3PO_4 model (Fig. S17).

In these studies, two O-H bonds were oriented away from the substrate to mimic plausible catalyst:substrate interaction modes for a surface-bound hydrogen phosphate group. Since most of the systems contain rotatable bonds, conformational sampling at every step in the mechanism was necessary.[38] Additionally, we explicitly considered the different energetics of diastereomeric species: commercially available **2,3-BDO** is obtained as a mixture of diastereomers, and several putative reaction intermediates can also exist as diastereomers. Only the energy values for the (*R*,*R*)-**2,3-BDO** stereoisomer are displayed since the (*R*,*S*) analogous presents similar energy profiles (Fig. S16), which is in high agreement with previous experimental work.[9].

Our calculations revealed a complex network of possible reaction pathways (Figs. S8-11), from which a high number of pathways have been overlooked in previous literature.[9,10] The most favorable pathway leading from **2,3-BDO** to **BDE** is shown in Fig. 4. The overall mechanism consists of an epoxide-mediated dehydration reaction accompanied by a second dehydration involving the nucleophilic addition of the catalyst. In the three TSs, the catalyst molecule promotes reactivity by enabling a concerted bifunctional proton transfer,[64] whereby a proton is transferred to the substrate from the acidic P-O-H group while another proton is accepted from the substrate by the P = O group. Initially, the mechanism starts with an epoxide-forming intramolecular nucleophilic substitution (from **2,3-BDO** to **BDO_EPOX_TS**, with an activation barrier ($\Delta G^{\ddagger}$) of 54.5 kcal·mol^{-1}), followed by an E2 reaction involving epoxide opening (from **B2EPOX** to **EPOX_E2_TS**, $\Delta G^{\ddagger}$ of 49.7 kcal·mol^{-1}) (Fig. 4). Then, intermediate 3-butene-2-ol (**3B2OL**) undergoes an S_N2' process (from **3B2OL** to **3B2OL_S_N2'_TS**, $\Delta G^{\ddagger}$ of 56.8 kcal·mol^{-1}) with a subsequent E2 elimination to produce the final **BDE** product (from **2B1P** to **2B1P_E2_TS**, $\Delta G^{\ddagger}$ of 43.9 kcal·mol^{-1}). The S_N2' reaction (**3B2OL_S_N2'_TS**) involves O–C bond formation between the substrate and phosphate catalyst. Due to the proximity of the SiO_2 support and the reacting substrate, **3B2OL_S_N2'_TS** might be less stable in the heterogeneous catalyst than in the H_3PO_4 model employed for the computational analysis. Therefore, alternative pathways from **3B2OL** to **BDE** might become more relevant than the S_N2' process in the real catalytic system, such as the direct E2 elimination (from **3B2OL** to **3B2OL_E2_TS**, $\Delta G^{\ddagger}$ of 60.2 kcal·mol^{-1}, Fig. S8).

The computational results reveal significant differences from previous proposals. To the best of our knowledge, the epoxide intermediate **B2EPOX** was never considered as a part of the primary catalytic cycle. Instead, it was considered a side-product.[10,65] Furthermore, previous mechanistic proposals have suggested that the dehydration processes

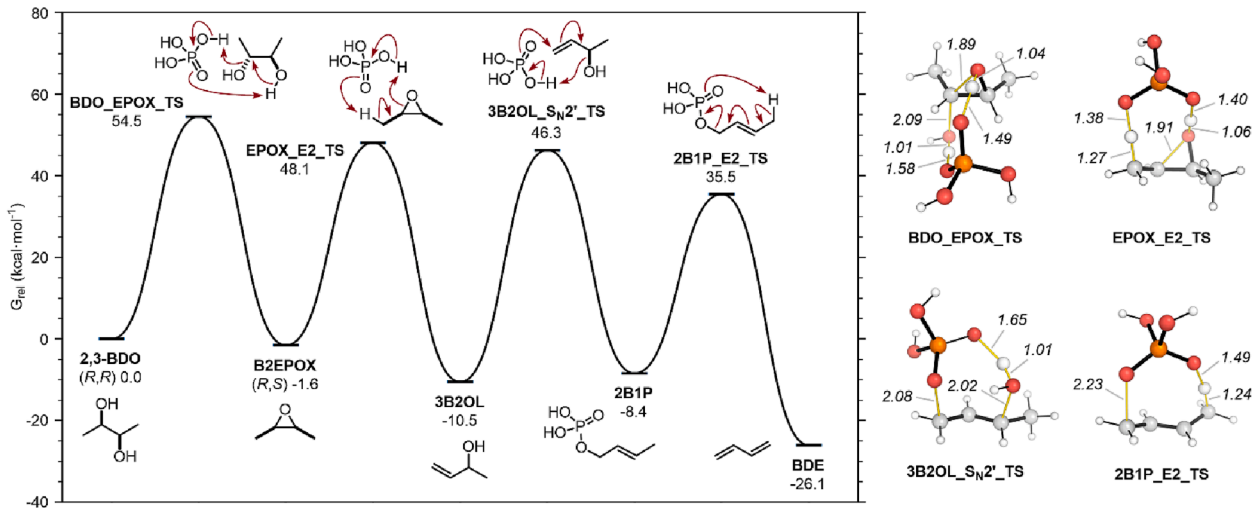

Fig. 4. Most favorable computed pathway to generate BDE from 2,3-BDO. Ensemble-averaged relative Gibbs energies in kcal·mol^{-1}. Forming and breaking bonds (in Å) are represented with thin yellow lines. C atoms in grey, H atoms in white, O atoms in red, and P atoms in orange. H_3PO_4 was used as the model catalyst. All QM results discussed below were obtained with the DLPNO-CCSD(T)/cc-pV(TQ)Z//M06-2X-D3/6–31 + G(d,p)[49–63] method at T = 623.15 K; quantitatively similar reaction profiles were obtained at other levels of theory (Fig. S4-7 vs. S8-11).

occur in two separate steps, involving carbocations (through OH elimination followed by deprotonation) [65–68], carbanions (through deprotonation followed by OH elimination) [12], or through step-wise bifunctional activation.[69] In contrast, the proposal presented in this work introduces a novel concept of dehydration mechanisms that proceed via concerted dehydration activated by bifunctional acid-base catalysis.

2.3. Analysis of key intermediates and competitive pathways

In line with our theoretical results, epoxide intermediate **B2EPOX** was previously observed and isolated experimentally; however, it was instead considered an off-cycle side-product that does not lie en route to **BDE** formation.[10] In contrast, our theoretical results suggest that **B2EPOX** is an on-cycle intermediate. We therefore set out to test this prediction experimentally: when **B2EPOX** was used as starting material **BDE** was the major product formed (Fig. 5A). For this, 5.24 wt% **B2EPOX** in H_2O flowed over both catalysts with varied liquid and helium gas flow rates. A maximum yield of 70C% **BDE** was produced from CsH_2PO_4/SiO_2 at the lower partial pressure of **B2EPOX** and higher residence time.

Importantly, the yields obtained ranged from 56 to 70C%, which is similar to the yields observed when **2,3-BDO** was used as the starting material, further strengthening that the epoxide is a short-lived species that forms during the main reaction pathway. Demonstration that **B2EPOX** is a catalytically-competent intermediate under standard reaction conditions, along with our computed energy profile, suggests that previously proposed unstable carbocations[9] can be bypassed. As seen in previous studies, no stable carbocations were found after **2,3-BDO** dehydration in any of the calculations due to spontaneous H and Me shifts that irreversibly lead to methyl ethyl ketone (**MEK**) and isobutyraldehyde (**IBA**).[66] Additionally, several compounds were collected from the liquid condenser, including **3B2OL**, **MEK** and 2-butene-1-ol (**2B1OL**) over the CsH_2PO_4/SiO_2 catalyst (Fig. 5B). Fig. 6A shows that all these side-products were also observed when using **2,3-BDO** as the starting material. The proportions of the side-products exhibit similar trends from **B2EPOX** to **2,3-BDO**, with **MEK** (44% C) being the major side-product, followed by **3B2OL** (34% C), **2B1OL** (19% C), and **IBA** (2% C). These results demonstrate that the same set of side-products is generated when switching the starting reagents, suggesting that **B2EPOX** is part of the proposed catalytic pathway.

Concurrently, **B2EPOX** was observed in the condensable products from **2,3-BDO** dehydration reactions (Fig. 6B), further suggesting that this epoxide is part of the main reaction pathway. Additional organic side products and intermediates were also detected experimentally, including acetoin, **MEK**, **IBA**, and **3B2OL** (Fig. 6). Varying the residence time in the flow reactor shifts the composition of the condensable products. To demonstrate this effect, an experiment was performed with increased weight hourly space velocity values and residence times compared to the experiments shown in Fig. 3. For this, **2,3-BDO** flowed over the CsH_2PO_4/SiO_2catalyst at flow rates of 0.017 or 0.034 g/min, and the diluent gas (N_2) flowed over the catalyst bed at 110 or 220 cm^3 (STP) min^{-1} at 400 °C and 1 atm. At a residence time of 0.95 s, a trace amount of **IBA** is seen in addition to 22C% **3B2OL** and 36C% **MEK** (Fig. 6A). However, at a residence time of 0.48 s, 2 C% **B2EPOX** is present, **MEK** concentration is reduced to 29C%, and **3B2OL** concentration increases to 41C% (Fig. 6B). The presence of **B2EPOX** and the increased concentration of **3B2OL** at a lower residence time is consistent with these species being key intermediates for **BDE** formation.

A detailed reaction mechanism including the major side products and potential catalyst inhibition pathways is presented in Fig. 7 and Figs. S8-11. Reaction selectivity is kinetically controlled since we found the competitive processes to be irreversible, based on successively lower TS stabilities along the reaction coordinate. Even though quantitative selectivity is not attainable due to different mass recovery in the gas and liquid phases and the use of a model catalytic system, the predicted amounts of each product agree qualitatively with experimental results: **BDE** and **MEK** are the major products ($\Delta G^{\ddagger}$ of 56.8 and 57.8 kcal·mol^{-1} for **BDE** and **MEK**, respectively, Fig. 7, right). Notably, the concentration of **3B2OL** was high in the experimental outcomes, which agrees with the calculated energy profile that shows **3B2OL** as a stable intermediate (-10.5 kcal·mol^{-1}) and supports that the S_N2' reaction taking place from **3B2OL** to **2B1P** is the rate-limiting step (RLS) of the main pathway for **BDE** production ($\Delta G^{\ddagger}$ of 56.8 kcal·mol^{-1}). Furthermore, the concentration of **B2EPOX** was very low in the experimental measurements, confirming that this species is a short-lived intermediate ($\Delta G^{\ddagger}$ from **B2EPOX** to **3B2OL** is only 49.7 kcal·mol^{-1}).

Ketonic species such as **MEK** and **IBA** are common side products obtained (Fig. 6). Our calculations suggest that these species are formed through hydrogen and methyl shifts (Fig. 8). As observed for the main pathway, the most favorable TSs leading to side-products involve bifunctional activation (i.e., P-O-H acidity and P = O Brønsted or Lewis basicity) from the H_3PO_4 catalyst. In line with the experimental results in Fig. 6, **MEK** is predicted to be the main side-product over **IBA** ($\Delta G^{\ddagger}$ of

A

Catalyst	P_{B2EPOX} (kPa)	Residence time (s)	**BDE** yield (C%)
CsH_2PO_4/SiO_2	0.27	0.95	70
CsH_2PO_4/SiO_2	0.45	0.92	62
CsH_2PO_4/SiO_2	0.25	0.48	56
H_3PO_4/SiO_2	0.24	0.94	31
H_3PO_4/SiO_2	0.38	0.94	32
H_3PO_4/SiO_2	0.25	0.48	31

B

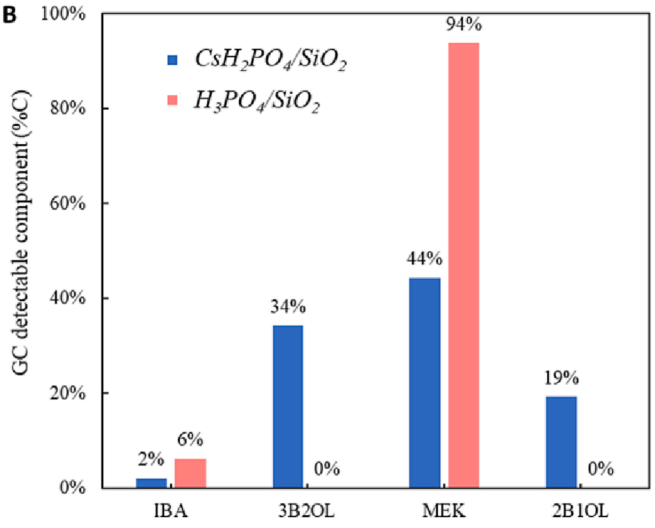

Fig. 5. (A) **BDE** production using the CsH_2PO_4/SiO_2 and H_3PO_4/SiO_2 catalysts from **B2EPOX** feed. Conditions: 0.02–0.04 mL min^{-1} feed containing 5.24 wt% **B2EPOX** in H_2O, 1 atm with 110–220 cm^3 (STP) min^{-1} of helium flow at 400 °C. (B) Condensable products recovered from **B2EPOX** conversion reactions.

57.8 and 60.1 kcal·mol^{-1} for **MEK** and **IBA**, respectively, Fig. 8). As with the main product-forming pathway, these side products are able to form without the intervention of carbocation intermediates.

2.4. QM/MM study of the catalytic center

With the information gathered using the H_3PO_4 model, hybrid QM/MM calculations were then used to computationally model key steps in the reaction mechanism with a larger silica slab, with the ONIOM method for a more realistic catalytic system. We focused on the most stable pathways located with the smaller model system. After optimizing the structure using QM/MM, we obtained a silica-supported phosphate catalyst with Cs that resembles the experimental catalytic site more than the previous H_3PO_4 model. We then reinvestigated the RLSs that lead to the two main products of the reaction, the S_N2' reaction taking place from **3B2OL** to **2B1P** (producing **BDE**) and the H shift from (*R*,*R*)-**2,3-BDO** to **MEK** (generating **MEK**) (Fig. 7). The activation barrier of 48.5 kcal·mol^{-1} for **BDE** formation obtained with this more realistic system (Fig. 9A) corresponds to a reaction half-life of 4.7 min at 400 °C.[70] This result is reasonably close to the experimental rates, which employed residence times in the scale of seconds.

To compare CsH_2PO_4- and H_3PO_4-supported catalysts, similar structures were employed in both cases. The selectivity differences of

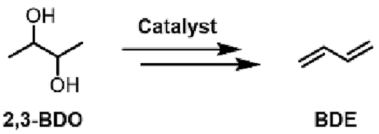

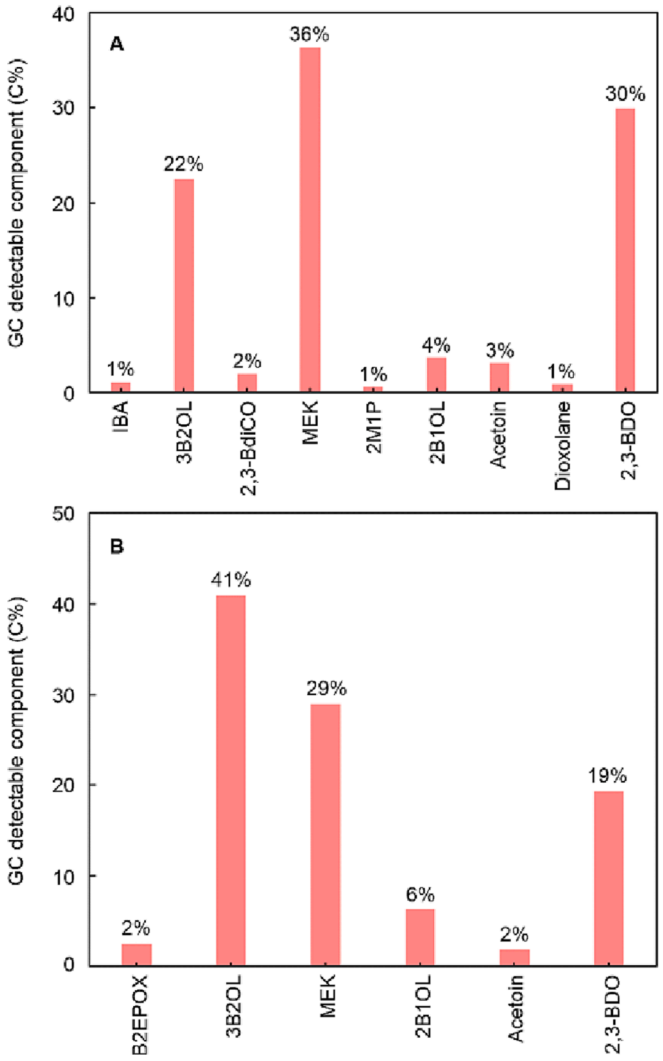

Fig. 6. Organic component distribution in condensable products from **2,3-BDO** dehydration with CsH_2PO_4/SiO_2 catalyst at two different residence times and equivalent partial pressures of **2,3-BDO**. (A) 2.0 g catalyst, 0.017 g/min **2,3-BDO**, 1 atm N_2 at 110 cm^3 (STP) min^{-1}, 400 °C. (B) 2.0 g catalyst, 0.034 g/min **2,3-BDO**, 1 atm N_2 at 220 cm^3 (STP) min^{-1}, 400 °C. **2,3-BdiCO** = 2,3-butanedione. **2M1P** = 2-methyl-1-propanol.

both types of catalysis were qualitatively studied using the corresponding RLSs for **BDE** and **MEK** generation. When using CsH_2PO_4/SiO_2 as the catalyst (Fig. 9A, C), the generation of **BDE** is favored over the formation of **MEK** (enthalpy activation barriers, $\Delta H^{\ddagger}$, of 48.5 vs. 49.8 kcal·mol^{-1}, $\Delta\Delta H^{\ddagger}$ of 1.3 kcal·mol^{-1}, **BDE**:**MEK** selectivity of 2.6:1 at 400 °C), which is in line with the experimental results. However, when the system studied switches to H_3PO_4/SiO_2 (Fig. 9B, D), the selectivity profile changes notably, and **MEK** is marginally preferred ($\Delta H^{\ddagger}$ of 47.4 vs. 47.0 kcal·mol^{-1}, $\Delta\Delta H^{\ddagger}$ of −0.4 kcal·mol^{-1}, **BDE**:**MEK** selectivity of 0.7:1 at 400 °C). This switch in reactivity is in high agreement with previously reported results,[9] which show a sharp drop in **BDE**:**MEK** selectivity when using the H_3PO_4/SiO_2 catalyst with no Cs centers (10 % CsH_2PO_4/SiO_2 shows **BDE**:**MEK** selectivity of 6.3:1 and 10 %H_3PO_4/SiO_2 leads to **BDE**:**MEK** selectivity of 1.1:1). Importantly, H_3PO_4/SiO_2 showed higher conversion and, therefore, faster experimental reactivity

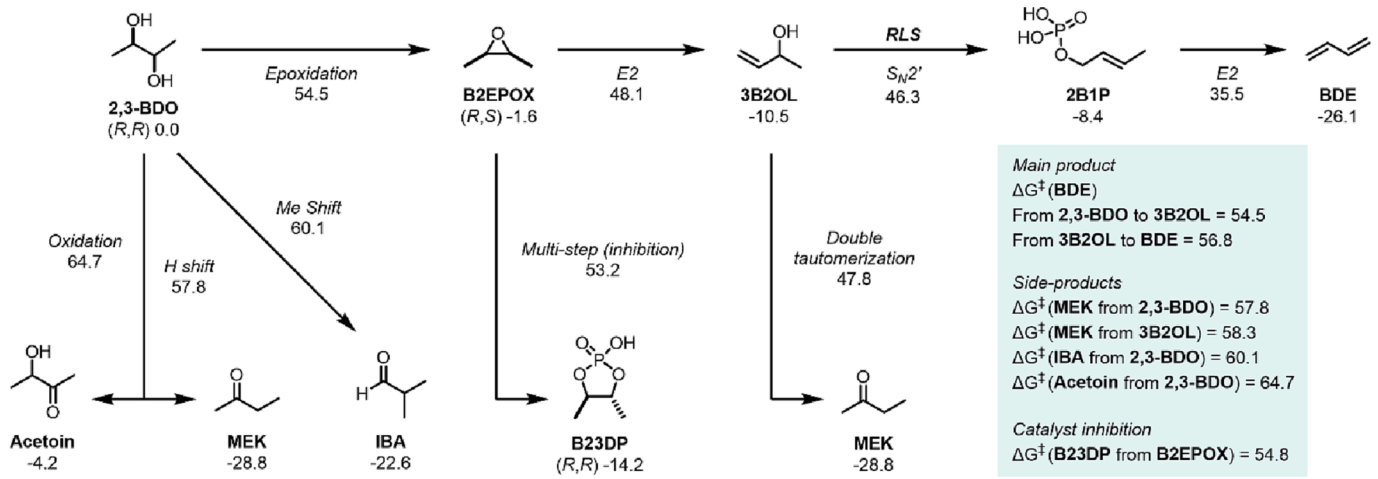

Fig. 7. Summary of the main pathways included in the H_3PO_4/SiO_2-catalyzed synthesis of **BDE** with their corresponding relative Boltzmann weighted relative G (in kcal·mol^{-1}) and the $\Delta G^{\ddagger}$ associated to the generation of the main product and side products, as well as catalyst inhibition. H_3PO_4 was used as the model catalyst.

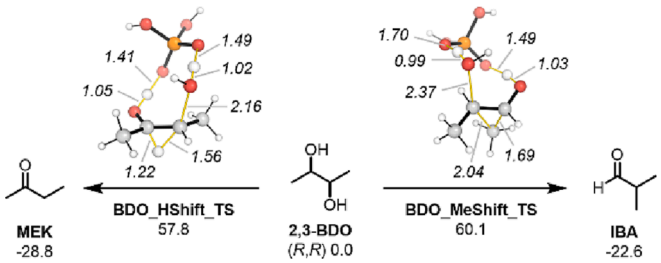

Fig. 8. Pathways to generate **MEK** and **IBA** from **2,3-BDO** and representations of the TSs involved, including relative Boltzmann weighted relative *G* (in kcal·mol^{-1}). HShift = hydrogen shift. MeShift = methyl shift. Forming and breaking bonds (in Å) are represented with thin yellow lines and the H atoms involved in these bonds are enlarged. H_3PO_4 was used as the model catalyst.

than CsH_2PO_4/SiO_2.[9] This observation agrees with the increase in the TS barriers calculated after Cs inclusion (from 47.4 to 48.5 kcal·mol^{-1}, Fig. 9A, B, and from 47.0 to 49.8 kcal·mol^{-1}, Fig. 9C, D).

To understand the differences in product preference, we examined multiple structural and electronic properties of the catalytic sites of CsH_2PO_4/SiO_2 and H_3PO_4/SiO_2. Previous proposals have suggested that the size of the metal cation influences reactivity and selectivity through steric interactions with the substrate. However, as seen in Fig. 9A, C, the Cs cation is oriented away from the approach of the substrate, such that its steric influence upon key intermediates and transition structures is minimal. In contrast, we observe electronic differences in the reactive phosphate groups: Natural population analysis (NPA)[71] charges of O atoms of the phosphate in CsH_2PO_4/SiO_2 are more negative than those found in the H_3PO_4/SiO_2 system (-1.23/-1.23/-1.01 vs. −1.15/-1.05/-0.99 for CsH_2PO_4/SiO_2 and H_3PO_4/SiO_2, respectively) (Fig. 9E, F). Greater negative charge on the phosphate oxygen atoms in the Cs-exchanged catalyst results in greater Brønsted basicity and nucleophilicity. Consistent with this hypothesis, in the S_N2' process representing the RLS during **BDE** formation, an earlier TS structure is obtained for CsH_2PO_4/SiO_2 vs. H_3PO_4/SiO_2 (forming C-O distance of 1.55 vs 1.20 Å) indicative of a more nucleophilic oxygen. The importance of a larger cationic radius is in reducing the covalency (and weakening) of O-M bonding, creating more electron-rich phosphate groups. The larger variation in $\Delta H^{\ddagger}$ when the Cs center is included is found in the H shift TS that leads to **MEK** (from 47.0 to 49.8 kcal·mol^{-1}, Fig. 9C, D). The main difference between the H shift and S_N2' TSs rely on the roles of the catalytic O atoms: while the H shift involves a basic O atom (Fig. 9C, D), the analogous O atom in the S_N2' process acts as a nucleophile (Fig. 9A, B). Therefore, the sharper energy change found for the H shift after adding Cs might be caused by a more significant increase in the basicity of the catalyst compared to its increment in nucleophilicity.

The acidity and basicity of the CsH_2PO_4/SiO_2 and H_3PO_4/SiO_2 catalysts were measured using temperature-programmed desorption (TPD) of ammonia and carbon dioxide. Following the protocol reported by Filimonov and coworkers,[10] helium was used to create an inert atmosphere in the TPD experiments. In line with the previously reported data, our results show that the basicity of the catalyst increases upon Cs incorporation (total basicity of 26 and 12 $\mu mol_{CO2} \cdot g^{-1}$ for CsH_2PO_4/SiO_2 andH_3PO_4/SiO_2, respectively, Fig. 9G) while acidity decreases (total acidity of 28 and 95 $\mu mol_{CO2} \cdot g^{-1}$ for CsH_2PO_4/SiO_2 and H_3PO_4/SiO_2, respectively). Previously, Filimonov and coworkers performed an extensive study regarding TPD of MH_2PO_4/SiO_2 derivatives,[10] showing temperature-programmed desorption curves of multiple catalysts during consecutive heating and cooling cycles. In this work, the authors also found that an increase in Cs concentration led to higher CO_2 absorption. The theoretical and experimental results suggests that the metal center acts as an electronic modulator that changes the basic/acid properties of the active catalytic centers, affecting reactivity and selectivity of the process.

3. Conclusion

The CsH_2PO_4-catalyzed **BDE** production from **2,3-BDO** was studied using experimental and computational techniques. The synthesized catalysts contained a 10 wt% loading of CsH_2PO_4 on SiO_2, which reduced the catalyst surface area by ~ 30% without significant pore volume change. STEM-EDS analysis revealed that both Cs and P were widely distributed across the SiO_2 support without forming large agglomerates. ^{31}P NMR experiments suggest that most of the phosphate species deposited onto the surface of CsH_2PO_4/SiO_2 exist as mono- or pyrophosphate groups. The catalyst was initially tested in a continuous flow reaction using commercially available **2,3-BDO**, leading to a maximum **BDE** yield of 63C%.

An intensive computational mechanistic study using H_3PO_4 as the model catalyst revealed that the reaction mainly proceeds through an epoxide-forming nucleophilic substitution leading to **B2EPOX** followed by an E2 reaction involving epoxide opening. Then, the resulting intermediate **3B2OL** undergoes an S_N2' process (rate-limiting step) with a subsequent E2 elimination to produce the final **BDE** product. These findings were supported experimentally since **BDE** was the major product obtained when **B2EPOX** was used as the starting material. Additionally, using QM/MM, we modeled a more realistic reactive system that included the SiO_2 support to study the effect of the metal center

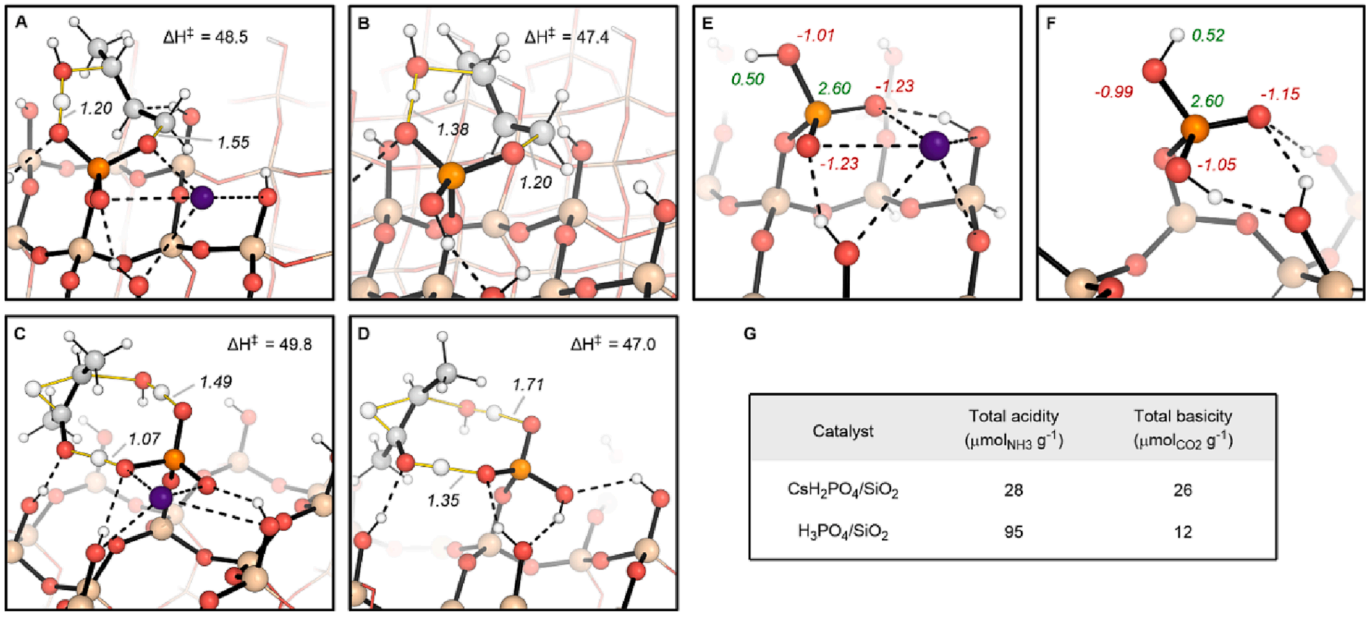

Catalyst	Total acidity ($\mu mol_{NH3}\ g^{-1}$)	Total basicity ($\mu mol_{CO2}\ g^{-1}$)
CsH_2PO_4/SiO_2	28	26
H_3PO_4/SiO_2	95	12

Fig. 9. (A-D) Comparison of TSs modeled with QM/MM for **BDE** (A, B) and **MEK** (C, D) production using CsH_2PO_4/SiO_2 (A, C) and H_3PO_4/SiO_2 (B, D) as the catalyst. $\Delta H^{\ddagger}$ in kcal·mol^{-1}. QM layer: M06-2X/def2-QZVPP//M06-2X/6–31 + G(d,p), def2-SVP for Cs only for geometry optimization; MM layer: UFF. The QM layer is represented with colored balls (H = white; C = grey; O = red; P = orange; Si = light brown; Cs = purple) and black sticks, while the MM layer is represented as colored sticks. Bonds involved in the TSs and hydrogen bonds are represented as yellow and dotted black lines, respectively. Distances are shown in Å. (E-F) Natural charges for relevant atoms in CsH_2PO_4/SiO_2 (E) and H_3PO_4/SiO_2 (F). Green and red numbers represent positive and negative charges, respectively. (G) Acid and base site densities for the CsH_2PO_4/SiO_2 and H_3PO_4/SiO_2 catalysts measured through temperature-programmed desorption of NH_3 (acid sites) and CO_2 (base sites).

on the catalysis. An NPA study showed that the O atoms of the phosphate are more negatively charged in CsH_2PO_4/SiO_2 than in H_3PO_4/SiO_2. This result suggests that the improved selectivity achieved when adding the metal center is related to an increase in the basicity of the catalyst. Temperature-programmed desorption experiments using CO_2 also show that the basicity of the catalyst increases upon Cs incorporation, strengthening the computational hypothesis.

This work presents novel concerted bifunctional catalytic mechanisms that from previous approaches based on carbocations and carbanions. This mechanism involves H transfers from the phosphate units, and the acidity and basicity of the catalyst play a crucial role in determining **BDE** yields. This parameter can be modulated with metal centers, which is important for designing catalysts that are basic enough to deprotonate OH groups while protonating leaving water molecules during dehydration processes. Additionally, on-cycle intermediate epoxide **B2EPOX** has been identified, which will aid in designing catalytic systems as this product was previously considered to be an innocuous side-product.

Declaration of Competing Interest

The authors declare that they have no known competing financial interests or personal relationships that could have appeared to influence the work reported in this paper.

Data availability

Data will be made available on request.

Acknowledgments

R.S.P. and J.V.A.-R. acknowledge the RMACC Summit supercomputer, supported by the NSF (ACI-1532235 and ACI1532236), and the Extreme Science and Engineering Discovery Environment (XSEDE) allocations TG-CHE180056 and TG-CHE200033. J.V.A.-R. acknowledges financial support through the Gobierno de Aragón-Fondo Social Europeo (Research Group E07_23R) and a Juan de la Cierva Incorporación contract from the Ministry of Science and Innovation (MCIN) and the State Research Agency (AEI) of Spain, and the European Union (NextGenerationEU/PRTR) under grant reference IJC2020-044217-I. S.K. acknowledges XSEDE allocation TG-CHE210034 and the National Renewable Energy Laboratory Computational Science Center. This work was authored in part by the National Renewable Energy Laboratory, managed and operated by Alliance for Sustainable Energy, LLC, for the U.S. Department of Energy (DOE) under Contract No. DE-AC36-08GO28308. Funding was provided by U.S. Department of Energy Office of Energy Efficiency and Renewable Energy Bioenergy Technologies Office and in collaboration with the Consortium for Computational Physics and Chemistry (CCPC) and the Chemical Catalysis for Bioenergy Consortium (ChemCatBio). G.R.H., X.H., F.G.B, K.A.U., B.C.K., R.E.D., and D.R.V. acknowledge funding from the Chemical Catalysis for Bioenergy consortium by the Bioenergy Technologies Office in the DOE Office of Energy Efficiency and Renewable Energy. Microscopy was performed in collaboration with the Chemical Catalysis for Bioenergy Consortium under contract no. DE-AC05-00OR22725 with Oak Ridge National Laboratory (ORNL) and through a user project supported by ORNL's Center for Nanophase Materials Sciences (CNMS), which is sponsored by the Scientific User Facilities Division, Office of Basic Energy Sciences, U.S. Department of Energy. Part of the microscopy research was also supported by the Office of Nuclear Energy, Fuel Cycle R&D Program and the Nuclear Science User Facilities. Authors thank Shawn K. Reeves for assistance with TEM sample preparation. We would also like to thank Stephen Tifft for his support on spinning band distillation, as well as Rick Elander and Min Zhang for their support and discussions regarding BDO fermentation. The views expressed in the article do not necessarily represent the views of the DOE or the U.S. Government. The U.S. Government retains and the publisher, by accepting the article for publication, acknowledges that the U.S. Government retains a non-exclusive, paid-up, irrevocable, worldwide license to publish or reproduce the published form of this work, or allows others to do so, for U.S. Government purposes. The results and analysis presented in this paper were partially possible thanks to the access

granted to computing resources at the Galicia Supercomputing Center, CESGA, including access to the FinisTerrae supercomputer, the Red Española de Supercomputación (grant number QH-2023-1-0003) and the Drago cluster facility of SGAI-CSIC.

Appendix A. Supplementary data

Supplementary data to this article can be found online at https://doi.org/10.1016/j.cej.2023.143346.

References

[1] E.V. Makshina, M. Dusselier, W. Janssens, J. Degrève, P.A. Jacobs, B. Sels, Review of old chemistry and new catalytic advances in the on-purpose synthesis of butadiene, Chem. Soc. Rev. 43 (2014) 7917–7953, https://doi.org/10.1039/C4CS00105B.

[2] N.L. Morrow, The industrial production and use of 1,3-butadiene, Environ. Health Perspect. 86 (1990) 7–8, https://doi.org/10.1289/ehp.90867.

[3] R.J. Dhanorkar, S. Mohanty, V.K. Gupta, Synthesis of functionalized styrene butadiene rubber and its applications in SBR–silica composites for high performance tire applications, Ind. Eng. Chem. Res. 60 (2021) 4517–4535, https://doi.org/10.1021/acs.iecr.1c00013.

[4] A. Kumar, S. Mohanty, V.K. Gupta, Butadiene rubber: synthesis, microstructure, and role of catalysts, Rubber Chem. Technol. 94 (2021) 393–409, https://doi.org/10.5254/rct.21.79948.

[5] Y. Qi, Z. Liu, S. Liu, L. Cui, Q. Dai, J. He, W. Dong, C. Bai, Synthesis of 1,3-butadiene and its 2-substituted monomers for synthetic rubbers, Catalysts 9 (2019) 97, https://doi.org/10.3390/catal9010097.

[6] K. Isobe, K. Sawai, K. Kawamura, K. Yamada and H. Yanase, Method for producing 2,3-butanediol, PCT Int. Appl. WO 2015/076279, 2015.

[7] S. Yang, A. Mohagheghi, M.A. Franden, Y.-C. Chou, X. Chen, N. Dowe, M. E. Himmel, M. Zhang, Metabolic engineering of *Zymomonas mobilis* for 2,3-butanediol production from lignocellulosic biomass sugars, Biotechnol. Biofuels 9 (2016) 189, https://doi.org/10.1186/s13068-016-0606-y.

[8] Z. Yang, Z. Zhang, Recent advances on production of 2,3-butanediol using engineered microbes, Biotechnol. Adv. 37 (2019) 569–578, https://doi.org/10.1016/j.biotechadv.2018.03.019.

[9] D. Tsukamoto, S. Sakami, M. Ito, K. Yamada, T. Yonehara, Production of bio-based 1,3-butadiene by highly selective dehydration of 2,3-butanediol over SiO_2-supported cesium dihydrogen phosphate catalyst, Chemistry Lett. 45 (2016) 831–833, https://doi.org/10.1246/cl.160309.

[10] W. Kim, W. Shin, K.J. Lee, Y. Cho, H.S. Kim, I. Filimonov, 2,3-Butanediol dehydration catalyzed by silica-supported alkali phosphates, Appl. Catal. A: Gen. 570 (2019) 148–163, https://doi.org/10.1016/j.apcata.2018.08.015.

[11] M. Huchede, T.T.N. Nguyen, L. Cardenas, M. Aouine, K. Jaillardon, J.-M.-M. Millet, Structure Sensitivity of 2,3-Butanediol Dehydration to Butadiene over Rare Earth Orthophosphate Catalysts, J. Phys. Chem. C 124 (2020) 2060–2069, https://doi.org/10.1021/acs.jpcc.9b10784.

[12] K. Nakazono, R. Takahashi, Y. Yamada, S. Sato, Dehydration of 2,3-butanediol to produce 1,3-butadiene over Sc_2O_3 catalyst prepared through hydrothermal aging, Mol. Catal. 516 (2021), 111996, https://doi.org/10.1016/j.mcat.2021.111996.

[13] X. Liu, V. Fabos, S. Taylor, D.W. Knight, K. Whiston, G.J. Hutchings, One-Step Production of 1,3-Butadiene from 2,3-Butanediol Dehydration, Chem. Eur. J. 22 (2016) 12290–12294, https://doi.org/10.1002/chem.201602390.

[14] H. Duan, Y. Yamada, S. Sato, Efficient production of 1,3-butadiene in the catalytic dehydration of 2,3-butanediol, App. Catal. A Gen. 491 (2015) 163–169, https://doi.org/10.1016/j.apcata.2014.12.006.

[15] Q. Zheng, J. Xu, B. Liu, K.L. Hohn, Mechanistic study of the catalytic conversion of 2,3-butanediol to butenes, J. Catal. 360 (2018) 221–239, https://doi.org/10.1016/j.jcat.2018.01.034.

[16] F.P. Lossing, J.L. Holmes, Stabilization energy and ion size in carbocations in the gas phase, J. Am. Chem. Soc. 106 (1984) 6917–6920, https://doi.org/10.1021/ja00335a008.

[17] J.-L.-M. Abboud, I. Alkorta, J.Z. Davalos, P. Müller, E. Quintanilla, J.-C. Rossier, Influence of carbocation stability in the gas phase on solvolytic reactivity: beyond bridgehead derivatives, J. Org. Chem. 68 (2003) 3786–3796, https://doi.org/10.1021/jo026539s.

[18] M. Caricato, Cluster model simulations of metal-doped amorphous silicates for heterogeneous catalysis, J. Phys. Chem. C 125 (2021) 27509–27519, https://doi.org/10.1021/acs.jpcc.1c07524.

[19] L. Simón, R.S. Paton, QM/MM study on the enantioselectivity of spiroacetalization catalysed by an imidodiphosphoric acid catalyst: how confinement works, Org. Biomol. Chem. 14 (2016) 3031–3039, https://doi.org/10.1039/C6OB00045B.

[20] P.M. Zimmerman, M. Head-Gordon, A.T. Bell, Selection and Validation of Charge and Lennard-Jones Parameters for QM/MM Simulations of Hydrocarbon Interactions with Zeolites, J. Chem. Theory Comput. 7 (2011) 1695–1703, https://doi.org/10.1021/ct2001655.

[21] C.E. Botez, J.D. Hermosillo, J. Zhang, J. Qian, Y. Zhao, J. Majzlan, R.R. Chianelli, C. Pantea, High-temperature phase transitions in CsH_2PO_4 under ambient and high-pressure conditions: A synchrotron x-ray diffraction study, J. Chem. Phys. 127 (19) (2007) 194701.

[22] Y. Taninouchi, T. Uda, Y. Awakura, Dehydration of CsH_2PO_4 at temperatures higher than 260 °C and the ionic conductivity of liquid product, Solid State Ion. 178 (2008) 1648–1653, https://doi.org/10.1016/j.ssi.2007.10.017.

[23] B.L. Turner, N. Mahieu, L.M. Condron, Phosphorus-31 Nuclear Magnetic Resonance Spectral Assignments of Phosphorus Compounds in Soil NaOH–EDTA Extracts, Soil Sci. Soc. Am. J. 67 (2003) 497–510, https://doi.org/10.2136/sssaj2003.4970.

[24] R.W. Mcdowell, I. Stewart, Peak assignments for phosphorus-31 nuclear magnetic resonance spectroscopy in pH range 5–13 and their application in environmental samples, Chem. Ecol. 21 (2005) 211–226, https://doi.org/10.1080/02757540500211590.

[25] P. Zhao, B. Boekfa, T. Nishitoba, N. Tsunoji, T. Sano, T. Yokoi, M. Ogura, M. Ehara, Theoretical study on ^{31}P NMR chemical shifts of phosphorus-modified CHA zeolites, Micropor. Mesopor. Mater. 294 (2020), 109908, https://doi.org/10.1016/j.micromeso.2019.109908.

[26] E.C. de O. Lima, J.M.M. Neto, F.Y. Fujiwara, F. Galembeck, Aluminum polyphosphate thermoreversible gels: a study by ^{31}P and ^{27}Al NMR spectroscopy, J. Colloid Interface Sci. 176 (1995) 388–396, https://doi.org/10.1006/jcis.1995.9953.

[27] L. Zhang, H. Eckert, Multinuclear NMR studies on the sol-gel preparation of sodium aluminophosphate glasses, Solid State, NMR 26 (2004) 132–146, https://doi.org/10.1016/j.ssnmr.2004.03.002.

[28] L. Montagne, G. Palavit, M. Draoui, Mechanism of polyphosphate gel formation in the Na_2O Al_2O_3 $_P2_O5$ system, J. Non-Cryst. Solids 155 (1993) 115–121, https://doi.org/10.1016/0022-3093(93)91315-T.

[29] Q. Zheng, M.D. Wales, M.G. Heidlage, M. Rezac, H. Wang, S.H. Bossmann, K. L. Hohn, Conversion of 2,3-butanediol to butenes over bifunctional catalysts in a single reactor, J. Catal. 330 (2015) 222–237, https://doi.org/10.1016/j.jcat.2015.07.004.

[30] D. Song, Kinetic model development for dehydration of 2,3-butanediol to 1,3-butadiene and methyl ethyl ketone over an amorphous calcium phosphate catalyst, Ind. Eng. Chem. Res. 55 (2016) 11664–11671, https://doi.org/10.1021/acs.iecr.6b02930.

[31] D. Song, Development of a deactivation model for the dehydration of 2,3-butanediol to 1,3-butadiene and methyl ethyl ketone over an amorphous calcium phosphate catalyst, Ind. Eng. Chem. Res. 56 (2017) 11013–11020, https://doi.org/10.1021/acs.iecr.7b02355.

[32] F. Zeng, S.H. Bossmann, M.G. Heidlage, K.L. Hohn, Transformation of 2,3-butanediol in a dual bed catalyst system, Chem. Engineer. Sci. 175 (2018) 387–395, https://doi.org/10.1016/j.ces.2017.10.009.

[33] N.T.T. Nguyen, F. Matei-Rutkovska, M. Huchede, K. Jaillardon, G. Qingyi, C. Michel, J.M.M. Millet, Production of 1,3-butadiene in one step catalytic dehydration of 2,3-butanediol, Catal. Today 323 (2019) 62–68, https://doi.org/10.1016/j.cattod.2018.07.007.

[34] Gaussian 16, Revision B.01, Gaussian, Inc., Wallingford CT, 2016 (full reference available in the ESI).

[35] ORCA, version 4.0.1.2, F. Neese, The ORCA Program System, WIREs Comput, Mol. Sci. 2 (2012) 73–78, https://doi.org/10.1002/wcms.81.

[36] F. Neese, Software update: The ORCA program system, version 4.0, WIREs Comput, Mol. Sci. 8 (2018) e1327.

[37] GoodVibes, version 2.0.3, G. Luchini, J. V. Alegre-Requena, I. Funes-Ardoiz and R. S. Paton, GoodVibes: Automated Thermochemistry for Heterogeneous Computational Chemistry Data, F1000Research 9 (2020) 291. https://doi.org/10.12688/f1000research.22758.1.

[38] AQME, version 1.3.0, J. V. Alegre-Requena, S. Sowndarya, T. Alturaifi, R. Pérez-Soto and R. S. Paton, AQME: Automated Quantum Mechanical Environments for Researchers and Educators. Wiley Interdiscip. Rev. Comput. Mol. Sci. (2023). https://doi.org/10.1002/wcms.1663.

[39] R.A. Van Santen, Theory of Brønsted acidity in zeolites, Stud. Surf. Sci. Catal. 85 (1994) 273–294, https://doi.org/10.1016/S0167-2991(08)60771-5.

[40] J.B. Nicholas, Density functional theory studies of zeolite structure, acidity, and reactivity, Topics Catal. 4 (1997) 157–171, https://doi.org/10.1023/A:1019179903977.

[41] J.A. Ryder, A.K. Chakraborty, A.T. Bell, Density functional theory study of proton mobility in zeolites: proton migration and hydrogen exchange in ZSM-5, J. Phys. Chem. B 104 (2000) 6998–7011, https://doi.org/10.1021/jp9943427.

[42] D.H. Wells Jr, W.N. Delgass Jr, K.T. Thomson, Evidence of defect-promoted reactivity for epoxidation of propylene in titanosilicate (TS-1) catalysts: a DFT study, J. Am. Chem. Soc. 126 (2004) 2956–2962, https://doi.org/10.1021/ja037741v.

[43] X. Solans-Monfort, C. Coperet, O. Eisenstein, Shutting down secondary reaction pathways: the essential role of the pyrrolyl ligand in improving silica supported d0-ML4 alkene metathesis catalysts from DFT calculations, J. Am. Chem. Soc. 132 (2010) 7750–7757, https://doi.org/10.1021/ja101597s.

[44] S. Kim, D.J. Robichaud, G.T. Beckham, R.S. Paton, M.R. Nimlos, Ethanol dehydration in HZSM-5 studied by density functional theory: Evidence for a concerted process, J. Phys. Chem. A 119 (2015) 3604–3614, https://doi.org/10.1021/jp513024z.

[45] C.M. Smith, N. Venkataraman, M.T. Gallagher, D. Müller, J.A. West, N.F. Borrelli, D.C. Allan, K.W. Koch, Low-loss hollow-core silica/air photonic bandgap fibre, Nature 424 (2003) 657–659, https://doi.org/10.1038/nature01849.

[46] M. Lazzeri, F. Mauri, First-principles calculation of vibrational Raman spectra in large systems: Signature of small rings in crystalline SiO_2, Phys. Rev. Lett. 90 (2003), 036401, https://doi.org/10.1103/PhysRevLett.90.036401.

[47] K. Suzuki, T. Noda, G. Sastre, N. Katada, M. Niwa, Periodic density functional calculation on the Brønsted acidity of modified Y-type zeolite, J. Phys. Chem. C 113 (2009) 5672–5680, https://doi.org/10.1021/jp8104562.
[48] S. Bailleul, I. Yarulina, A.E.J. Hoffman, A. Dokania, E. Abou-Hamad, A. D. Chowdhury, G. Pieters, J. Hajek, K. De Wispelaere, M. Waroquier, J. Gascon, V. A. Van Speybroeck, A Supramolecular View on the Cooperative Role of Brønsted and Lewis Acid Sites in Zeolites for Methanol Conversion, J. Am. Chem. Soc. 141 (2019) 14823–14842, https://doi.org/10.1021/jacs.9b07484.
[49] G.D. Purvis III, R.J. Bartlett, A Full Coupled-cluster singles and doubles model: the inclusion of disconnected triples, J. Chem. Phys. 76 (1982) 1910–1918, https://doi.org/10.1063/1.443164.
[50] J.A. Pople, M. Head-Gordon, K. Raghavachari, Quadratic configuration interaction. A general technique for determining electron correlation energies, J. Chem. Phys. 87 (1987) 5968–5975, https://doi.org/10.1063/1.453520.
[51] C. Riplinger, F. Neese, An efficient and near linear scaling pair natural orbital based local coupled cluster method, J. Chem. Phys. 138 (3) (2013) 034106.
[52] C. Riplinger, B. Sandhoefer, A. Hansen, F. Neese, Natural triple excitations in local coupled cluster calculations with pair natural orbitals, J. Chem. Phys. 139 (13) (2013) 134101.
[53] C. Riplinger, P. Pinski, U. Becker, E.F. Valeev, F. Neese, Sparse maps – a systematic infrastructure for reduced-scaling electronic structure methods. II. Linear scaling domain based pair natural orbital coupled cluster theory, J. Chem. Phys. 144 (2) (2016) 024109.
[54] T.H. Dunning Jr, Gaussian basis sets for use in correlated molecular calculations. I. The Atoms boron through neon and hydrogen, J. Chem. Phys. 90 (1989) 1007–1023, https://doi.org/10.1063/1.456153.
[55] D.E. Woon, T.H. Dunning Jr, Gaussian basis sets for use in correlated molecular calculations. III. The Atoms aluminum through argon, J. Chem. Phys. 98 (1993) 1358–1371, https://doi.org/10.1063/1.464303.
[56] E.R. Davidson, Comment on "Comment on Dunning's correlation-consistent basis sets", Chem. Phys. Lett. 260 (1996) 514–518, https://doi.org/10.1016/0009-2614(96)00917-7.
[57] W.J. Hehre, R. Ditchfield, J.A. Pople, Self-consistent molecular orbital methods. XII. Further extensions of gaussian-type basis sets for use in molecular orbital studies of organic molecules, J. Chem. Phys. 56 (1972) 2257–2261, https://doi.org/10.1063/1.1677527.
[58] P.C. Hariharan, J.A. Pople, The influence of polarization functions on molecular orbital hydrogenation energies, Theoret. Chim. Acta 28 (1973) 213–222, https://doi.org/10.1007/BF00533485.
[59] M.M. Francl, W.J. Pietro, W.J. Hehre, J.S. Binkley, M.S. Gordon, D.J. DeFrees, J. A. Pople, Self-consistent molecular orbital methods. XXIII. A polarization-type basis set for second-row elements, J. Chem. Phys. 77 (7) (1982) 3654–3665.
[60] V.A. Rassolov, M.A. Ratner, J.A. Pople, P.C. Redfern, L.A. Curtiss, 6–31G* basis set for third-row atoms, J. Comp. Chem. 22 (2001) 976–984, https://doi.org/10.1002/jcc.1058.
[61] T. Clark, J. Chandrasekhar, G.W. Spitznagel, P. von, R. Schleyer, Efficient diffuse function-augmented basis sets for anion calculations. III. The 3–21+G basis set for first-row elements, Li–F, J. Comput. Chem. 4 (1983) 294–301, https://doi.org/10.1002/jcc.540040303.
[62] Y. Zhao, D.G. Truhlar, The M06 suite of density functionals for main group thermochemistry, thermochemical kinetics, noncovalent interactions, excited states, and transition elements: two new functionals and systematic testing of four M06-class functionals and 12 other functionals, Theor. Chem. Acc. 120 (2008) 215–241, https://doi.org/10.1007/s00214-007-0310-x.
[63] S. Grimme, J. Antony, S. Ehrlich, H.A. Krieg, Consistent and accurate ab initio parameterization of density functional dispersion correction (DFT-D) for the 94 Elements H-Pu, J. Chem. Phys. 132 (2010), 154104, https://doi.org/10.1063/1.3382344.
[64] M.M. Cox, W.P. Jencks, Concerted bifunctional proton transfer and general-base catalysis in the methoxyaminolysis of phenyl acetate, J. Am. Chem. Soc. 103 (1981) 580–587, https://doi.org/10.1021/ja00393a014.
[65] W. Kim, W. Shin, K.J. Lee, H. Song, H.S. Kim, D. Seung, I.N. Filimonov, 2,3-Butanediol dehydration catalyzed by silica-supported sodium phosphates, App. Catal. A Gen. 511 (2016) 156–167, https://doi.org/10.1016/j.apcata.2015.11.043.
[66] A.G. Thome, N. Ayral, H. Toufar, T. Klüner, F. Roessner, Dehydration of 2,3-butanediol: a catalytical and theoretical approach, Catal. Lett. 147 (2017) 1271–1277, https://doi.org/10.1007/s10562-017-2027-3.
[67] J. Zhao, D. Yu, W. Zhang, Y. Hu, T. Jiang, J. Fu, H. Huang, Catalytic dehydration of 2,3-butanediol over P/HZSM-5: effect of catalyst, reaction temperature and reactant configuration on rearrangement products, RSC Adv. 21 (2016) 16988–16995, https://doi.org/10.1039/C5RA23251A.
[68] A. Matsuda, F. Sato, Y. Yamada, S. Sato, Efficient Production of 1,3-Butadiene from 1,4-Butanediol over Yb_2O_3 Catalyst Prepared through Hydrothermal Aging, Bull. Chem. Soc. Jpn. 95 (2022) 506–512, https://doi.org/10.1246/bcsj.20210457.
[69] H. Duan, Y. Yamada, S. Sato, Selective dehydration of 2,3-butanediol to 3-buten-2-ol over ZrO_2 modified with CaO, Applied Catalysis A, General 487 (2014) 226–233, https://doi.org/10.1016/j.apcata.2014.09.007.
[70] H. Eyring, The Activated Complex in Chemical Reactions, The Journal of Chemical Physics 3 (2) (1935) 107–115.
[71] E.D. Glendening, C.R. Landis, F. Weinhold, NBO 6.0: Natural bond orbital analysis program, J. Comput. Chem. 34 (16) (2013) 1429–1437.